Journal of Solid State Chemistry **144,** 35–44 (1999)
Article ID jssc.1998.8107, available online at http://www.idealibrary.com on IDEAL®

Crystal Structure of Sodium Rare Earth Oxyborates $Na_2Ln_2(BO_3)_2O$ (Ln = Sm, Eu, and Gd) and Optical Analysis of $Na_2Gd_2(BO_3)_2O:Eu^{3+}$

G. Corbel[1] and M. Leblanc

Laboratoire des Fluorures, UPRES-A 6010, Université du Maine, Avenue Olivier-Messiaen, 72085 Le Mans Cedex, France

and

E. Antic-Fidancev and M. Lemaître-Blaise

Laboratoire de Chimie Appliquée de l'Etat Solide, UMR 7574, ENSCP, 11, rue P. et. M. Curie, 75231, Paris Cedex 05, France

Received June 14, 1998; in revised form November 10, 1998; accepted November 22, 1998

A new structural family of rare earth oxyborates $Na_2Ln_2(BO_3)_2O$ (Ln = Sm, Eu and Gd) is evidenced. The structure, determined by single crystal X-ray diffraction, is monoclinic, space group $P2_1/c$, $Z = 4$, with $a = 10.695(6)$ Å, $b = 6.320(4)$ Å, $c = 10.328(6)$ Å, $\beta = 117.80(4)^\circ$, $V = 617.5(9)$ Å^3, $R_1 = 0.039$, w$R_2 = 0.101$ for $Na_2Gd_2(BO_3)_2O$. The three-dimensional network is built up from infinite sheets of LnO_8 polyhedra in the (b, c) plane, which are separated by sodium ions. The luminescence of trivalent europium in polycrystalline $Na_2Gd_2(BO_3)_2O:Eu^{3+}$ is analysed at 77K. The low symmetry of the rare earth sites, deduced from the X-ray diffraction study, is confirmed. The crystal field strength is high for both europium sites.

INTRODUCTION

In the search of UV transparent materials with SHG (second harmonic generation) and/or lasing properties, borates, oxyborates, or fluoride borates represent attractive candidates (1–5). Large crystals of oxyborate $Ca_4GdO(BO_3)_3$ (GdCOB) (6) are obtained by the Czochralski technique while borates β-BaB_2O_4 (BBO) (1), LiB_3O_5 (LBO) (2), or $YAl_3(BO_3)_4:Nd^{3+}$ (YAB) (3) and fluoride borate $KBe_2BO_3F_2$ (KBBF) (4) grow from melts.

Rare earth fluoride borates are unknown and we have recently undertaken the study of these mixed anionic systems. Decomposition, due to the formation of BF_3 gas, frequently occurs at high temperature. Consequently, crystallization must be performed at low temperature. A new structural family $Ln_3(BO_3)_2F_3$ (Ln = Sm, Eu, and Gd) (7) is now evidenced. However, fluoride-borate melts, which present a low viscosity, also favor the crystal growth of borates. This was demonstrated recently in the BaB_2O_4-BaF_2-2NaF-$Na_2B_2O_4$ system (8). Therefore, we report in this paper the synthesis and the structure determination of a new rare earth oxyborate family $Na_2Ln_2(BO_3)_2O$ (Ln = Sm, Eu, and Gd). The luminescence of $Na_2Gd_2(BO_3)_2O:Eu^{3+}$ is studied; the site symmetry is analyzed in connection with the crystal structure and the crystal field parameters are modelized by using Wybourne's formalism.

[1] To whom correspondence should be addressed.

EXPERIMENTAL

Single crystals of $Na_2Ln_2(BO_3)_2O$ grow from a mixture of $1B_2O_3$, $1Ln_2O_3$, $2LnF_3$, $6Na_2O$. This mixture is heated as follows: 6 h at 700°C, 15 h at 900°C for $Na_2Gd_2(BO_3)_2O$, or 15 h at 990°C for $Na_2Sm_2(BO_3)_2O$ and $Na_2Eu_2(BO_3)_2O$, and cooling at 0.1°C/min. Good quality powders are obtained by heating the stoichiometric mixture of $1B_2O_3$, $1Ln_2O_3$ and $1Na_2CO_3$ in platinum tubes. Weight losses, corresponding to the departure of CO_2, are observed.

Single crystals of $Na_2Gd_2(BO_3)_2O$ were selected by optical examination, and X-ray diffraction data (Table 1) were collected on a Siemens AED2 four-circle diffractometer. The crystal cell and the space group were obtained from long exposure rotation photographs. The conditions of intensity measurement are reported in Table 1. The scattering factors and anomalous dispersion corrections for all atoms were taken from the International Tables for X-ray Crystallography (9). Intensities were corrected for absorption with SHELX-76 (10). Structural calculations were performed with SHELXS-86 (11) and SHELXL-93 (12) programs. Structure projections were realized with the program Diamond (13).

The crystals of $Na_2Gd_2(BO_3)_2O$ were analyzed with a scanning electron microscope (SEM), Hitachi S2300,

0022-4596/99 $30.00

TABLE 1
Crystallographic Data and Conditions of Data Collection for $Na_2Gd_2(BO_3)_2O$

Crystal dimensions (mm^3)	$0.05 \times 0.12 \times 0.15$
Absorption (Mo$K\alpha$)	$\mu = 215.5\ cm^{-1}$
A_{max}, A_{min}	0.32, 0.10
Symmetry	Monoclinic
Space group	$P2_1/c$ (n°14)
Z	4
Parameters (293 K)	
a (Å)	10.695(6)
b (Å)	6.320(4)
c (Å)	10.328(6)
β (°)	117.80(4)
Volume (Å^3)	617.5(9)
Calculated density (g/cm^3)	5.31(1)
Secondary extinction factor	4.7(4) 10^{-6}
Weighting scheme	$k = 1$
$w = k/(\sigma^2(F^2) + (0.0719P)^2$	
Number of refined parameters	109
Max Δ/σ	0.002
Reliability factors R_1; wR_2	0.039; 0.101
Goodness of fit	1.02
Max, min heights in the final difference Fourier map (eÅ^{-3})	+ 4.9, − 4.8
Centering reflections ($2\Theta \approx 30°$)	27
Reflections for refined cell parameters	27 (scans at $\pm\Theta$)
Scan mode ω-2Θ in N steps of $\Delta\omega = 0.035°$	$37 \leq N \leq 43$
Data collection range	$2\Theta \leq 70°$
Aperture	4 × 4 mm
Measured reflections	2925
Minimum h, k, l; maximum h, k, l	− 15 0 0; 15 10 16
Standard reflections	1 0 4; 5 0 0; 4 2 − 2
Maximum standard intensity variation	2.8%
Independent reflections ($I > 2\sigma(I)$)	2169

equipped with a Link EDX spectrometer. The EDX analyses indicate sodium/oxygen and gadolinium/oxygen ratios close to 2/7 and the absence of fluorine.

The characterization of $Na_2Gd_2(BO_3)_2O$ was performed by coupled TGA-DTA thermal analysis under argon flow (TA Instruments SDT 2960, heating rate 10°C/min, temperature range 30–1300°C). Two successive weight losses of about 6% are observed above 750°C. The resulting products are Gd_2O_3 and probably B_2O_3 in the form of a glass. Consequently these weight losses may correspond to the departure of Na_2O in two steps.

The luminescence of trivalent europium in the powder sample $Na_2Gd_2(BO_3)_2O:Eu^{3+}$ (2%) was measured under the 457.9 nm blue line of a 5 W argon–ion laser at liquid-nitrogen temperature (77 K). A Rhodamine 6 G continuous-wave dye laser, pumped by the argon–ion laser, was used to excite selectively the $^5D_0$ level. The fluorescence emission was detected through a 1-m Jarrell Ash monochromator equipped with a Hamamatsu R374 photomultiplier.

STRUCTURE DETERMINATION AND DESCRIPTION

The structure determination was performed on $Na_2Gd_2(BO_3)_2O$. The conditions of systematic reflection lead to the $P2_1/c$ ($n°14$) centric space group, $h0l$: $l = 2n$, $0k0$: $k = 2n$. The starting set of atomic coordinates was obtained from the analysis of the Patterson map (Patt option of SHELXS-86 program (11)) and two heavy atoms were located on 4e crystallographic sites ($R_1 = 0.176$). The positions of all other atoms (Na, B, O) were given by successive refinements and Fourier difference syntheses (SHELXL-93). Finally, the refinements of anisotropic or isotropic (boron atoms) displacement parameters and secondary extinction factor converged to $R_1 = 0.039$ ($wR_2 = 0.101$).

The atomic coordinates and temperature factors are reported in Table 2, the anisotropic displacement parameters are given in Table 3, and the selected interatomic distances are listed in Table 4.

A valence bond analysis was tested by using the scheme proposed by Zachariasen (14) and Brown (15): the bond valence, s, is calculated as a function of interatomic distances, d_i, and summed over the coordination sphere of a given atom. The calculated Σs values for $Na_2Gd_2(BO_3)_2O$ (Table 5) are consistent with the proposed formulation.

It must be noted that the evolution of the cell parameters of samarium, europium and gadolinium compounds (Table 6) is in agreement with the variation of rare earth cationic radii.

Rare earth atoms occupy the center of distorted LnO_8 triangulated dodecahedra (bisdisphenoid) (Fig. 1). Sodium

TABLE 2
Atomic Coordinates and Temperature Factors in $Na_2Gd_2(BO_3)_2O$

Atom	Site	x	y	z	B_{eq} [Å^2][a]
Gd(1)	4e	0.18531(3)	0.08225(5)	0.08949(3)	0.39(1)
Gd(2)	4e	0.98249(3)	0.45948(5)	0.18103(3)	0.37(1)
Na(1)	4e	0.5229(3)	− 0.0573(5)	0.2624(4)	1.1(1)
Na(2)	4e	0.6094(4)	0.2622(7)	0.0469(4)	1.6(1)
O(1)	4e	0.9728(5)	0.1235(8)	0.0959(5)	0.5(1)
O(2)	4e	0.3179(5)	− 0.2556(8)	0.1359(6)	0.8(1)
O(3)	4e	0.1700(5)	0.2621(8)	0.3645(5)	0.6(1)
O(4)	4e	0.1504(5)	0.4594(8)	0.0877(6)	0.7(1)
O(5)	4e	0.3980(5)	0.162(1)	0.0552(5)	0.8(1)
O(6)	4e	0.8486(5)	0.2581(8)	0.2716(5)	0.7(1)
O(7)	4e	0.3727(6)	0.149(1)	0.3401(6)	1.0(1)
B(1)	4e	0.3183(7)	0.251(1)	− 0.0797(7)	0.51(8)[b]
B(2)	4e	0.2097(7)	− 0.347(1)	0.1496(8)	0.58(8)[b]

[a] $B_{eq} = \left(\frac{8\pi^2}{3}\right) \sum_i \sum_j U_{ij} a_i^* a_j^* a_i a_j$ (15).

[b] B_{iso}.

TABLE 3
Anisotropic Displacement Parameters in $Na_2Gd_2(BO_3)_2O$

Atom	U_{11}	U_{22}	U_{33}	U_{23}	U_{13}	U_{12}
Gd(1)	0.0062(1)	0.0038(2)	0.0061(2)	0.0000(1)	0.0027(1)	− 0.0001(1)
Gd(2)	0.0067(1)	0.0033(1)	0.0055(2)	0.0000(1)	0.0032(1)	0.0003(1)
Na(1)	0.013(2)	0.014(2)	0.017(2)	0.001(2)	0.005(2)	− 0.000(1)
Na(2)	0.017(2)	0.029(2)	0.018(2)	0.005(2)	0.010(2)	− 0.002(2)
O(1)	0.009(2)	0.006(2)	0.007(2)	− 0.001(2)	0.004(2)	0.001(2)
O(2)	0.011(2)	0.009(2)	0.016(2)	0.000(2)	0.009(2)	− 0.000(2)
O(3)	0.008(2)	0.010(2)	0.007(2)	0.002(2)	0.003(2)	0.000(2)
O(4)	0.012(2)	0.005(2)	0.012(2)	0.001(2)	0.007(2)	0.001(2)
O(5)	0.009(2)	0.015(2)	0.007(2)	0.004(2)	0.002(2)	0.001(2)
O(6)	0.011(2)	0.008(2)	0.009(2)	0.001(2)	0.005(2)	0.001(2)
O(7)	0.013(2)	0.016(2)	0.012(2)	− 0.004(2)	0.007(2)	0.001(2)

Note. The anisotropic temperature factor expression is: $T = \exp[-2\pi^2((ha^*)^2U_{11} + ... + 2hka^*b^*U_{12})]$ (16).

atoms Na(1) and Na(2) are sixfold and sevenfold coordinated, respectively. These coordinations are currently found in sodium–rare earth borates or sodium borates (18). The mean interatomic distances (Table 4) are in good agreement with the sum of ionic radii of Gd^{3+} (1.053 Å) or Na^+ (1.02 Å (VI), 1.12 Å (VII)) and O^{2-} (1.35 Å) (17). Boron atoms adopt a triangular coordination. The mean B-O distance, 1.38 Å, is close to that found generally in borates: $Ca_5(BO_3)_3F$, 1.38Å (19), $NaBe_2BO_3F_2$, 1.37Å (20), $NdAl_3(BO_3)_4$, 1.393Å (21), $Na_3Nd(BO_3)_2$, 1.378Å (18).

The structure can be described in terms of rare earth and sodium polyhedra. The three-dimensional network is built up from infinite sheets of $Ln O_8$ polyhedra in the (*b*,*c*) plane, which are separated by sodium ions along the *a* axis (Fig. 2). These layers are related by the inversion center at the center of the unit cell.

Two $Ln(1)O_8$ polyhedra share one edge in order to form $Ln(1)_2O_{14}$ dimers (Fig. 3). The arrangement of these dimeric entities can be described with a pseudo *F* face centered network (dashed lines in Fig. 3).

The $Ln(2)O_8$ polyhedra share triangular faces along *b* and form infinite zig-zag chains parallel to this axis (Fig. 4). These chains are joined together by edges in the (*b*,*c*) plane in order to build infinite $Ln(2)O_4$ layers (at $x = 0$) in which the $Ln(1)_2O_{14}$ dimers are inserted. The connection between *Ln*(1) and *Ln*(2) polyhedra is realized by edges. It must be noted that similar layers of ThI_8 distorted antiprisms, parallel to the (-101) plane, are found in ThI_4 (21a). In these layers, the ThI_8 polyhedra share one edge and two triangular faces (Fig. 5).

Borate groups are isolated one from another. They share edges or vertices with rare earth and sodium polyhedra (Fig. 2). Recently Grice *et al.* described several carbonates with layers of flat-lying, standing-on-base, standing-on-top, or standing-on-edge CO_3^{2-} triangles (22). It is interesting to note that, in $Na_2Ln_2(BO_3)_2O$, borate ions lie in infinite layers, parallel to the (*b*,*c*) plane. They form alternative rows, parallel to the *c* axis, of standing-on-base and standing-on-top BO_3^{3-} groups (Fig. 6).

ANALYSIS OF THE LUMINESCENCE SPECTRA

Nonselective argon–ion laser excitation ($\lambda_{exc} = 457.9$ nm) of polycrystalline $Na_2Gd_2(BO_3)_2O:Eu^{3+}$ (2%), was recorded at 77 K between 575 and 750 nm. The europium luminescence exhibits a complex emission spectrum (Fig. 7). It consists of several groups of narrow lines, attributed to the $^5D_0 \rightarrow {}^7F_{0-4}$ transitions of Eu^{3+}. The emission from higher ^5D_J levels ($J = 1$ and 2) is completely quenched, probably due to a multiphonon de-excitation process and the only emitting level is the lowest lying $^5D_0$ level of ^5D_J manifold. Two $^5D_0 \rightarrow {}^7F_0$ transitions are clearly evidenced at 17275 and 17264 cm^{-1} (Fig. 8). They correspond to two nonequivalent europium sites (A and B)

TABLE 4
Selected Interatomic Distances (Å) and Angles (°) in $Na_2Gd_2(BO_3)_2O$

Gd(1) polyhedron		Gd(2) polyhedron	
Gd–O(1)	2.279(4)	Gd–O(1)	2.282(3)
Gd–O(1)	2.319(5)	Gd–O(1)	2.363(3)
Gd–O(4)	2.411(4)	Gd–O(3)	2.371(6)
Gd–O(3)	2.458(5)	Gd–O(4)	2.401(6)
Gd–O(7)	2.461(4)	Gd–O(6)	2.407(7)
Gd–O(2)	2.483(5)	Gd–O(3)	2.413(5)
Gd–O(5)	2.511(6)	Gd–O(6)	2.498(5)
Gd–O(6)	2.622(5)	Gd–O(4)	2.512(6)
⟨Gd(1)–O⟩ = 2.44 Å		⟨Gd(2)–O⟩ = 2.41 Å	
Na(1) polyhedron		**Na(2) polyhedron**	
Na–O(2)	2.327(5)	Na–O(2)	2.354(8)
Na–O(5)	2.371(6)	Na–O(5)	2.387(7)
Na–O(5)	2.432(6)	Na–O(7)	2.498(5)
Na–O(2)	2.443(5)	Na–O(6)	2.528(4)
Na–O(7)	2.477(7)	Na–O(7)	2.677(7)
Na–O(7)	2.629(7)	Na–O(5)	2.871(7)
⟨Na(1)–O⟩ = 2.45 Å		Na–O(2)	2.995(7)
		⟨Na(2)–O⟩ = 2.62 Å	
Borate BO_3^{3-} ions			
B(1)–O(7)	1.366(8)	O(7)–B(1)–O(5)	124.5(4)
B(1)–O(5)	1.371(7)	O(5)–B(1)–O(3)	115.9(7)
B(1)–O(3)	1.415(8)	O(3)–B(1)–O(7)	119.6(6)
⟨B–O⟩ = 1.38 Å			
B(2)–O(2)	1.358(9)	O(2)–B(2)–O(4)	123.7(9)
B(2)–O(4)	1.389(6)	O(4)–B(2)–O(6)	116.9(5)
B(2)–O(6)	1.402(8)	O(6)–B(2)–O(2)	119.4(6

TABLE 5
Valence Bond Analysis of $Na_2Gd_2(BO_3)_2O$

	Gd(1)	Gd(2)	Na(1)	Na(2)	B(1)	B(2)	Σs	Expected
O(1)	0.561	0.556					2.067	2
	0.503	0.447						
O(2)	0.323		0.241	0.224		1.036	2.039	2
			0.176	0.039				
O(3)	0.346	0.437			0.888		2.061	2
		0.390						
O(4)	0.392	0.403				0.952	2.046	2
		0.299						
O(5)	0.300		0.214	0.205	1.000		1.955	2
			0.181	0.055				
O(6)	0.222	0.397		0.140		0.920	1.989	2
		0.310						
O(7)	0.343		0.160	0.152	1.014		1.868	2
			0.106	0.093				
Σs	2.990	3.239	1.078	0.908	2.902	2.908		
Expected	3	3	1	1	3	3		

B–O $s = \exp[(1.371 - d_i)/0.37]$ Na–O $s = \exp[(1.8 - d_i)/0.37]$
Gd–O $s = \exp[(2.065 - d_i)/0.37]$
(values from reference (15))

and confirm the rare earth environments found by crystallography.

In the monoclinic $P2_1/c$ space group, both rare earth ions occupy very low symmetry sites, C_1. According to group theory selection rules, all the electronic transitions are allowed and the degeneracy of each J level is completely lifted due to the crystal field Hamiltonian. A maximum of $2J + 1$ sublevels is expected for each ^7F_J level (1-3-5-7 and 9 lines for $J = 0$, 1, 2, 3, and 4 respectively).

The odd parameters of the crystal field lead to the significant oscillator strength of 0-0 transition (23). These electric dipole induced transitions are only allowed for C_s, C_n or C_{nv} symmetry. Their large intensity, related with the odd parameters, and the number of Stark components $(2J + 1)$ observed in the emission spectrum for almost all J levels of the ^7F_J manifold confirm the low symmetry of the europium sites in this sodium rare earth oxyborate.

In Fig. 7 three emission spectra of Eu^{3+} in $Na_2Gd_2(BO_3)_2O:Eu^{3+}$ are given in 575–730 nm wavelength range: (a) the nonselective argon ion–laser excitation ($\lambda_{exc} = 457.9$ nm); (b) dye laser excitation at $\lambda_{exc} = 578.88$ nm (site A), and (c) dye laser excitation at $\lambda_{exc} = 579.24$ nm (site B). These two last excitations correspond to the 0-0 transitions detected at 17275 and 17264 cm^{-1} under Ar^+ excitation and attributed to site A and to site B, respectively. In all the emission spectra, nonselective as well as dye selective excitations, the magnetic dipole $^5D_0 \rightarrow {}^7F_1$ transition and the $^5D_0 \rightarrow {}^7F_2$ electric dipole transition have high and similar intensities. For site A, the $^5D_0 \rightarrow {}^7F_4$ transition is also intense. There is no reasonable explanation for that particularity of the 0-1 magnetic dipole transition; however the same feature was observed recently in $Na_3Eu(CO_3)_3$ (24). In other borates, e.g. aragonite $LaBO_3:Eu^{3+}$ (25) or vaterite $LuBO_3:Eu^{3+}$ (26), the magnetic dipole transition $^5D_0 \rightarrow {}^7F_1$ is even stronger than the electric dipole transition 0-2. Blasse explains this phenomenon by the high energy of the charge transfer states which exalts the magnetic dipole transitions (27).

In Fig. 8, parts of luminescence spectra for $^5D_0 \rightarrow {}^7F_{0-4}$ transitions are collected for both Eu^{3+} sites. Two energy levels schemes are deduced from the optical data (Tables 7 and 8).

TABLE 6
Cell Parameters of $Na_2Ln_2(BO_3)_2O$ (*Ln* = Sm, Eu, and Gd)

	a (Å)	b (Å)	c (Å)	β (°)	V (Å^3)	R_i (Å)[a]
$Na_2Sm_2(BO_3)_2O$	10.754(2)	6.369(2)	10.381(2)	117.85(2)	628.6(2)	1.079
$Na_2Eu_2(BO_3)_2O$	10.721(7)	6.343(6)	10.347(7)	117.84(5)	622.1(6)	1.066
$Na_2Gd_2(BO_3)_2O$	10.695(6)	6.320(4)	10.328(6)	117.80(4)	617.5(9)	1.053

[a] Values from Ref. (17)

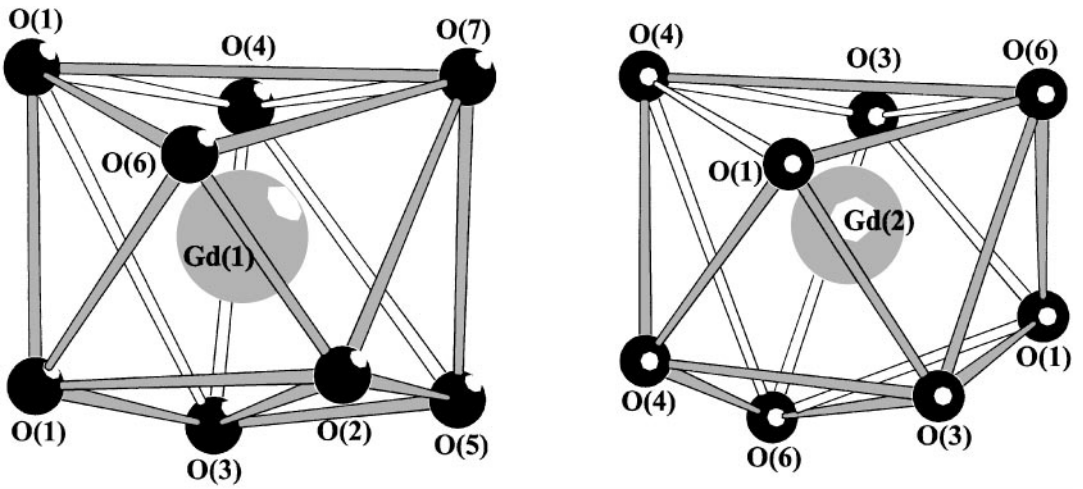

FIG. 1. Rare earth polyhedra in $Na_2Gd_2(BO_3)_2O$.

CRYSTAL FIELD SIMULATION

The parametric crystal field analysis was first performed for the C_{2v} symmetry instead of the C_1 site symmetry of Eu^{3+} in $Na_2Gd_2(BO_3)_2O:Eu^{3+}$. For the C_1 refinement, 27 crystal field parameters (cfp) are involved, and unfortunately only 17 (plus 2 uncertain) and 25 experimental ^7F_J sublevels are deduced, respectively, from the emission spectra of rare earth sites A and B. Therefore, the set is reduced to 9 real cfp in C_{2v} symmetry. It must be noted that the symmetry of the rare earth polyhedra is close to C_{2v} (Fig. 1).

According to Wybourne's formalism, the crystal field Hamiltonian can be expressed as

$$H_{cf} = \sum_{kq} [B_q^k (C_q^k + C_{-q}^k) + iS_q^k (C_q^k - C_{-q}^k)]$$

with B_q^k and S_q^k being the real and imaginary cfp and C_q^k the spherical harmonics. In the case of C_{2v} symmetry, the *cf*

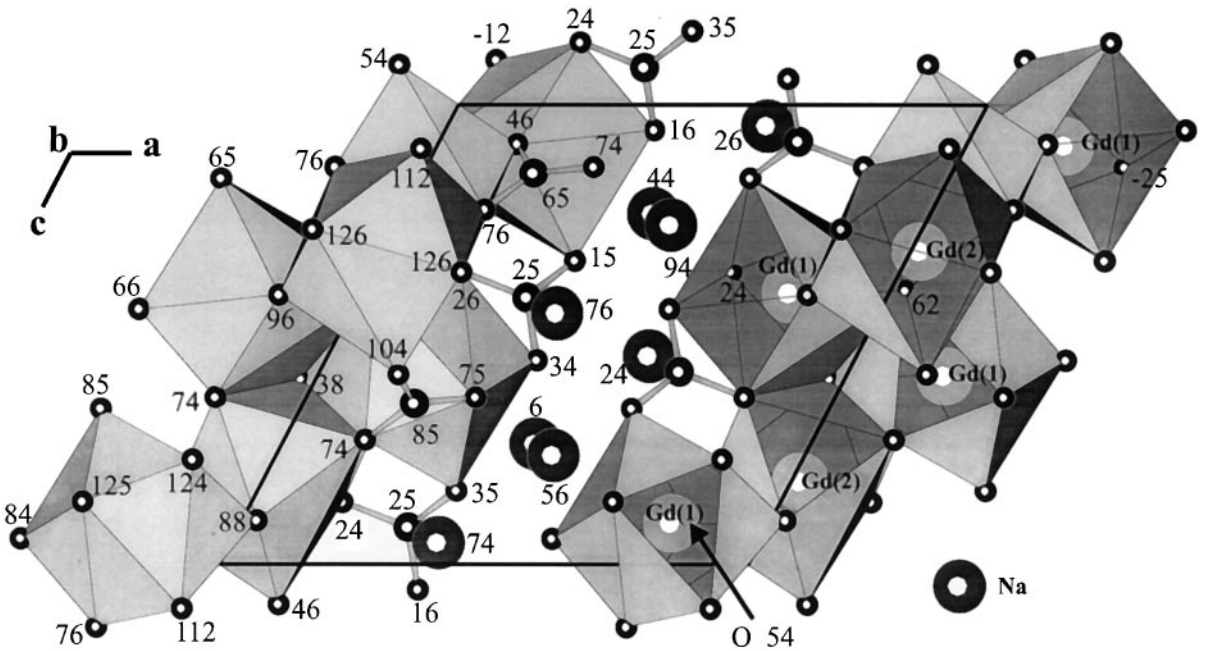

FIG. 2. Projection, on the (a, c) plane, of the structure of $Na_2Gd_2(BO_3)_2O$ with rare earth polyhedra, borate BO_3^{3-} groups, and sodium ions (coordinates along b in hundreds).

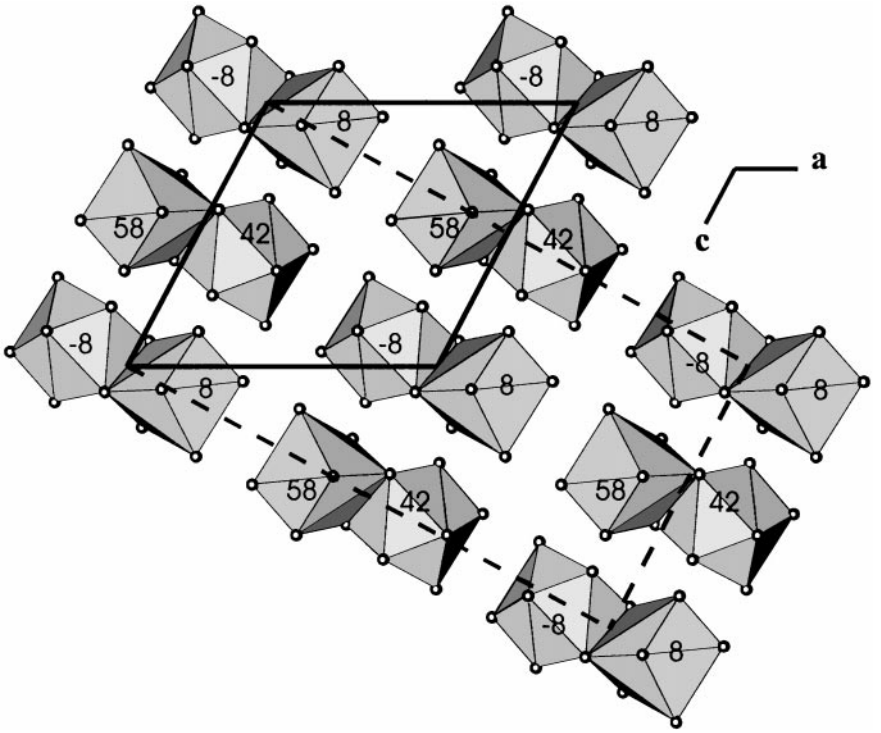

FIG. 3. Connection of the $Gd(1)O_8$ polyhedra and pseudo F centered network (in dashed lines) of $Gd(1)_2O_{14}$ groups (Gd coordinates along b in hundreds).

Hamiltonian is given by

$$H_{cf}(C_{2v}) = B_0^2 + B_0^4 + B_0^6 + B_2^2(C_2^2 + C_{-2}^2) + B_2^4(C_2^4 + C_{-2}^4) + B_2^6(C_2^6 + C_{-2}^6) + B_4^4(C_4^4 + C_{-4}^4) + B_4^6(C_4^6 + C_{-4}^6) + B_6^6(C_6^6 + C_{-6}^6).$$

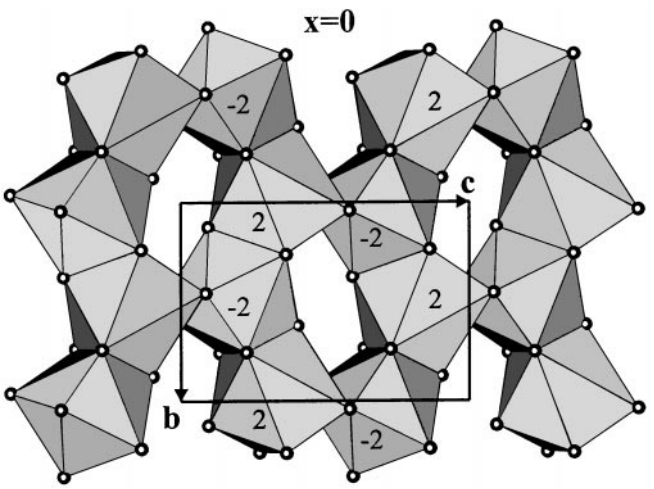

FIG. 4. Connection of the $Gd(2)O_8$ polyhedra (Gd coordinates along a in hundreds).

The calculation of the cfp of Eu^{3+} (ground configuration $4f^6$) can be efficiently performed on the reduced ^7F_J basis. It is due to the fact that the ground ^7F term is well isolated from the first excited ^5D term ($\Delta E \approx 12000\ cm^{-1}$) and also, that the crystal field operator allows the mixing of states of the same multiplicity. As nondiagonal spin–orbit interactions are neglected (small components of the ^5D_J levels into the ^7F_J wavefunctions), some "intermediate parameters" have been introduced, one for each ^7F_J level, which settle the experimental and calculated barycenters (28).

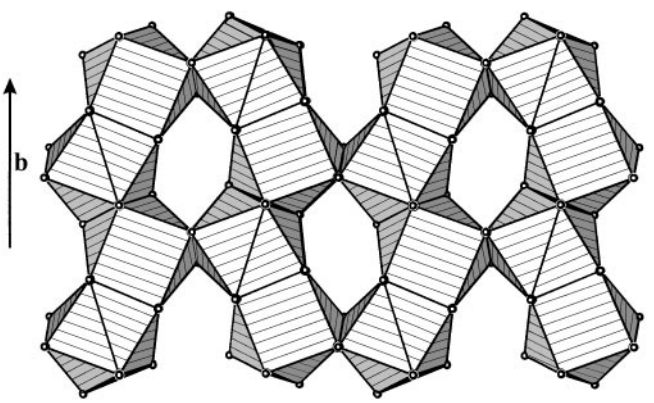

FIG. 5. Connection of the ThI_8 polyhedra in the (-101) plane of ThI_4.

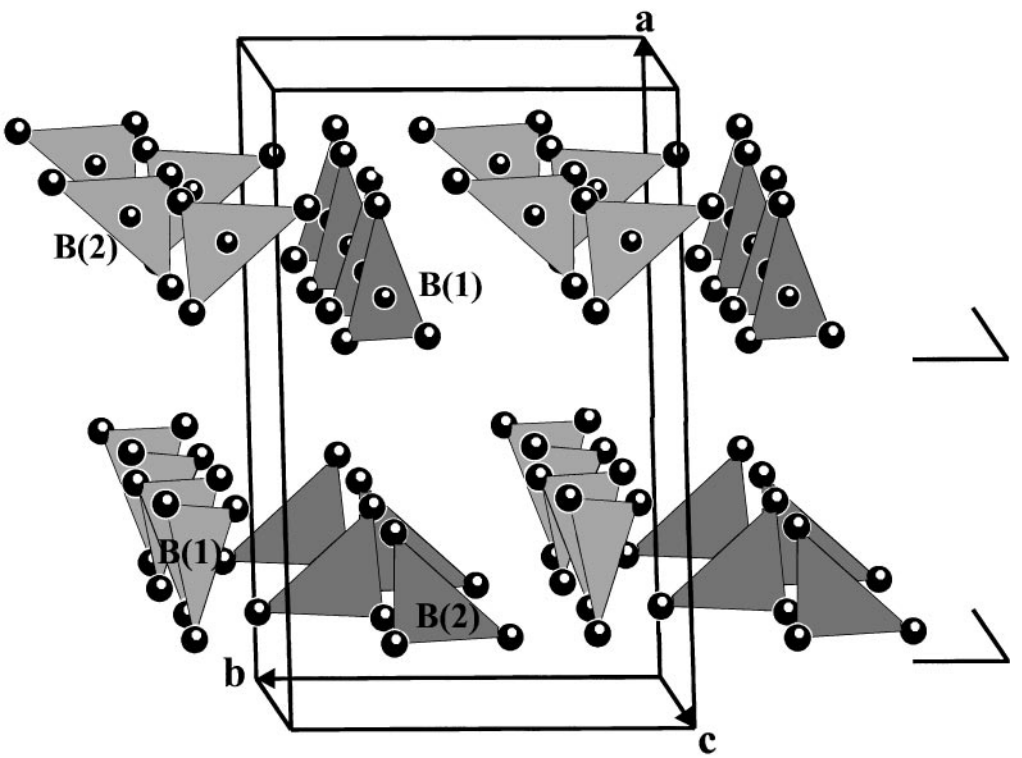

FIG. 6. Orientation of borate groups in $Na_2Gd_2(BO_3)_2O$.

To derive the cfp, we proceed in the following way: in the first step, the cfp of rank 2, being principally responsible for the splitting of the $^7F_1$ level, are calculated from the $^7F_1$ levels. In the second step, $B^2_{0,2}$ are kept constant and four rank cfp are refined from the $^7F_2$ levels. Then, the $^7F_{3-4}$ levels permit the derivation of six rank cfp.

In the case of site B, the simulation was performed without any particular problem: 1, 3, 5, 7, and 9 lines are

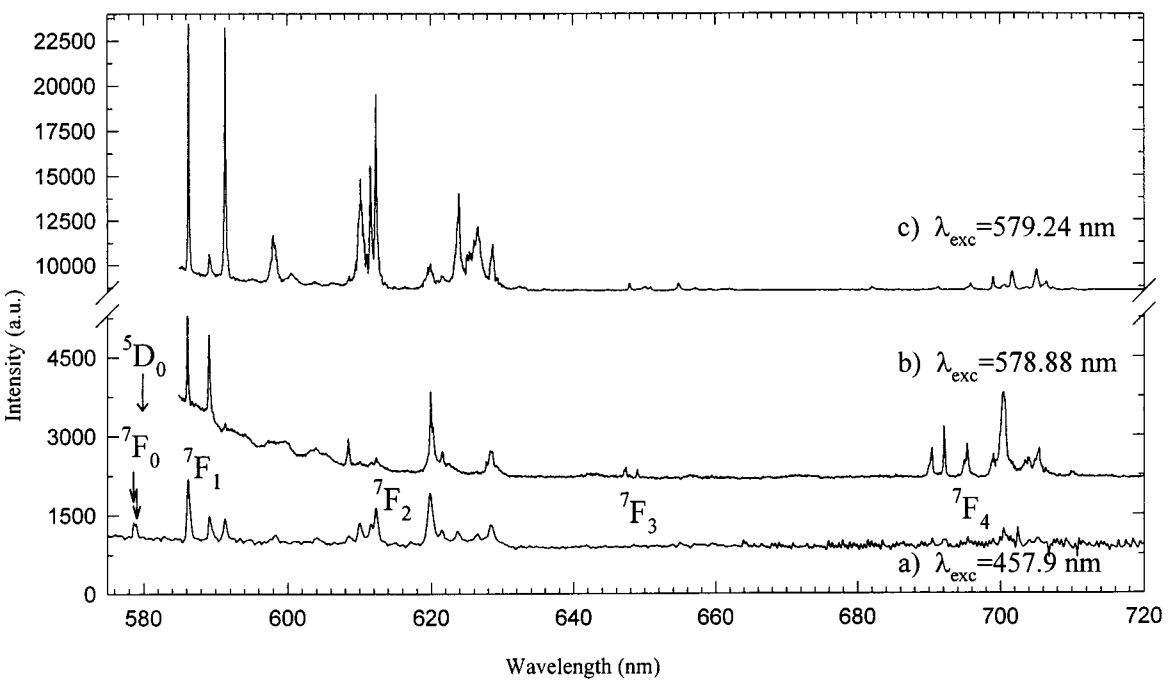

FIG. 7. Argon–ion laser and selective excitation of the europium emission in $Na_2Gd_2(BO_3)_2O:Eu^{3+}$ at 77 K.

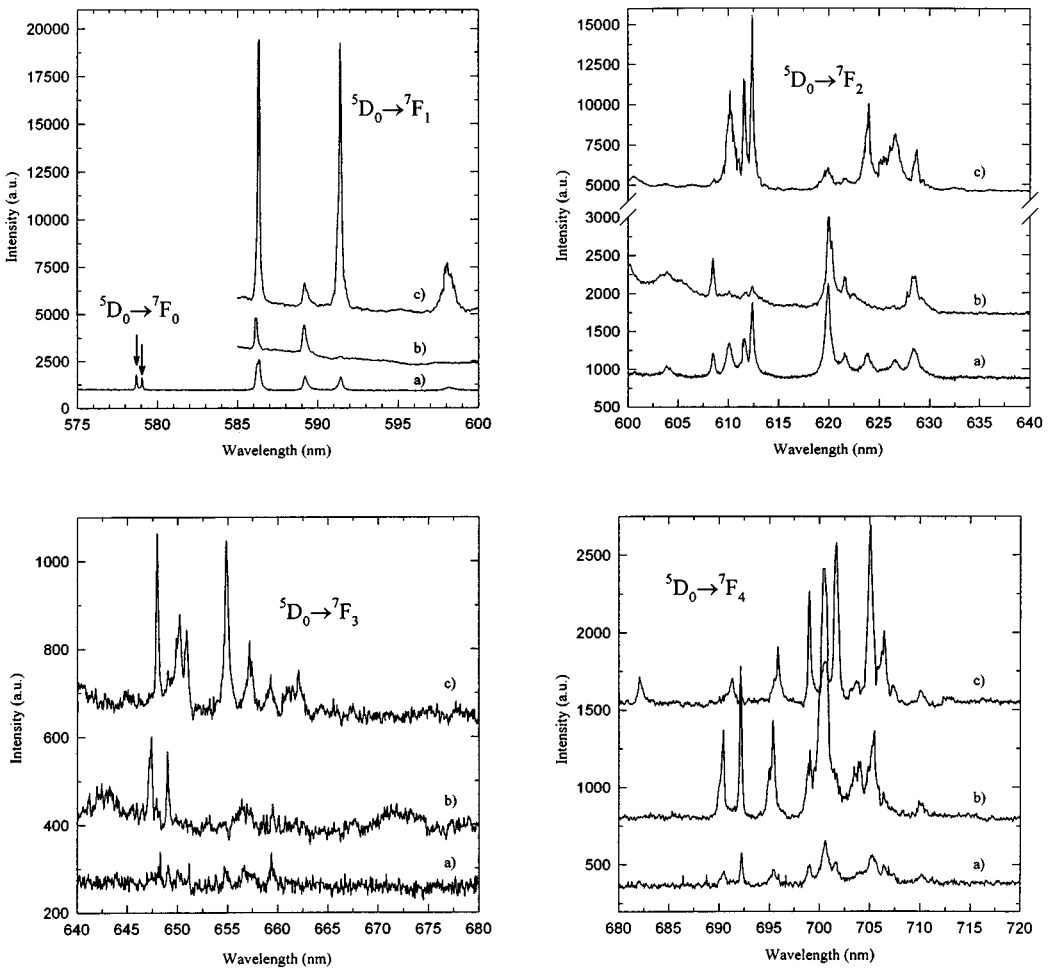

FIG. 8. Parts of luminescence spectra of Eu^{3+} in $Na_2Gd_2(BO_3)_2O:Eu^{3+}$ at 77 K under (a) argon–ion laser excitation at 457.9 nm, (b) dye excitation at 578.88 nm, (site A), (c) dye excitation at 579.24 nm (site B).

observed in the emission spectrum and assigned to $^7F_{0-4}$ levels. A very good rms deviation (12.8) is obtained. The best set of cfp is given in Table 9. A quite different situation exists for site A. For this site, only two lines are observed for the $^7F_1$ level under selective dye laser excitation. The third Stark component is supposed to be situated at 610 cm^{-1} (in fact, several broadbands are present in that domain, probably perturbed by phonon influence). With this statement, the $^7F_1$ barycenter of site A satisfies the generally accepted mean value, and the cfp of rank 2 can be derived. The same problem occurs for the $^7F_2$ level for which only four Stark components are detected in the emission spectrum. Referring to the $^7F_2$ barycenter value, the fifth Stark component may be the lowest one situated at about 720 cm^{-1}, probably also in the phonon bands. The presence of the highest $^7F_2$ sublevel at 1371 cm^{-1} implies that the overall splitting of these $^7F_2$ level is 651 cm^{-1}. This is one of the largest splittings found for Eu^{3+}. Moreover, it is very difficult to reproduce the experimental $^7F_2$ splitting by using the C_{2v} symmetry *cf* Hamiltonian and the results are not improved in C_1 symmetry: the rms deviation is bad (Table 9). Consequently, the assignment of the $^7F_2$ electronic levels for site A is questionable and it is possible that the transitions at 720 and 1371 cm^{-1} are due to phonon influence.

Then, a partial simulation of the crystal field parameters, limited to four rank cfp, is tentatively proposed for site A.

The values of the crystal field strength parameter, N_v, are large for both sites. N_v is calculated according to (29).

CONCLUSION

A new structural family of rare earth oxyborates $Na_2Ln_2(BO_3)_2O$ (Ln = Sm, Eu and Gd) is evidenced. The synthesis is achieved by solid state reaction and flux method. The monoclinic structure is determined by single

TABLE 7
Emission Lines of Eu^{3+} in $Na_2Gd_2(BO_3)_2O:Eu^{3+}$ (457.9 nm Argon–Ion Laser Excitation at 77 K)

Transition	E (cm^{-1})	Transition	E (cm^{-1})
$^5D_0 \rightarrow {}^7F_0$	17275	$^5D_0 \rightarrow {}^7F_3$	15422
	17264		15265
			15216
$^5D_0 \rightarrow {}^7F_1$	17052		15161
	17049		
	16967	$^5D_0 \rightarrow {}^7F_4$	14661
	16903		14481
	16713		14445
			14378
$^5D_0 \rightarrow {}^7F_2$	16555		14305
	16430		14273
	16386		14253
	16346		14205
	16325		14180
	16126		14158
	16084		14137
	16026		14082
	15956		
	15909		

crystal X-ray diffraction. LnO_8 polyhedra build infinite (100) sheets in which boron atoms are inserted in triangular coordination. These infinite sheets are separated by Na^+ ions.

TABLE 8
Experimental and Calculated Energy Levels (cm^{-1}) of Eu^{3+} Sites in $Na_2Gd_2(BO_3)_2O:Eu^{3+}$

	Site A		Site B	
$^{2S+1}L_J$ level	E exp.	E calc.	E exp.	E calc. Set I
$^7F_0$	0	0	0	0
$^7F_1$	223	204	215	219
	308	303	361	363
	(610)	630	551	541
$^7F_2$	(720)	735	878	894
	845	862	918	918
	1149	1127	939	930
	1191	1175	1238	1241
	(1366)	1375	1308	1306
$^7F_3$	1830		1834	1825
	1869		1887	1879
			1902	1918
			1995	1998
			2050	2046
			2098	2101
			2162	2158
$^7F_4$	—		2603	2619
	2792		2800	2795
	2827		2894	2874
	2894		2958	2938
	2998		3011	3004
	3061		3054	3062
	3071		3080	3094
	3099		3107	3126
	3191		3182	3176
$^5D_0$	17275		17264	

TABLE 9
Crystal Field Parameters and Crystal Field Strength Parameter N_v, for Eu^{3+} ions in $Na_2Gd_2(BO_3)_2O:Eu^{3+}$

B_q^k	Site A E (cm^{-1}) in C_1	Site B E (cm^{-1}) in C_{2v}
B_0^2	− 686	− 1098
B_2^2	686	386
B_0^4	2803	− 1665
B_2^4	− 378	560
S_2^4	1692	—
B_4^4	− 242	823
S_4^4	198	—
B_0^6		64
B_2^6		83
B_4^6		792
B_6^6		− 141
n°levels	9	25
σ	22.7	12.8
$N_{v,k=2}$	1883	1944
$N_{v,k=4}$	4431	2576
$N_{v,2+4}$	4815	3227
$N_{v,\text{total}}$		3418

The luminescence analysis of $Na_2Gd_2(BO_3)_2O:Eu^{3+}$ confirms the existence of two Eu^{3+} sites, in agreement with the crystallographic study. For one site, the *cfp* are easily calculated; for the other site, the line assignment is difficult and implies a very large and unexpected splitting of the $^7F_2$ sublevels. A partial simulation of the phenomenological crystal field parameters, significant for a large field strength for both sites, is proposed.

REFERENCES

1. C. Chen, B. Wu, A. Jiang, and G. You, *Scientia Sinica*, *B* **28,** 235 (1985).
2. C. Chen, Y. Wu, A. Jiang, B. Wu, G. You, R. Li, and S. Lin, *J. Opt. Soc. Am. B* **6,** 616 (1989).
3. T. Y. Fan and R. L. Byer, *IEEE J. Quant. Electr.* **24,** 895 (1988).
4. L. P. Solov'eva and V. V. Bakakin, *Kristallografija* **15,** 922 (1970).
5. R. Norrestam, M. Nygren, and J.-O. Bovin, *Chem. Mater.* **4,** 737 (1992)
6. G. Aka, A. Kahn-Harari, D. Vivien, J.-M. Benitez, F. Salin, and J. Godard, *Eur. J. Solid State Inorg. Chem.* **33,** 727 (1996).
7. G. Corbel, R. Retoux, and M. Leblanc, *J. Solid State Chem.* **139,** 52 (1998).
8. W. Zhuang, G. Rao, J. Liang, Y. Zhang, Y. Shi, Z. Qiao, and J. Shen, *J. Solid State Chem.* **126,** 80 (1996).
9. "International Tables for X-ray Crystallography," Vol. IV, Kynoch Press, Birmingham, (1968).
10. G. M. Sheldrick, "SHELX-76: Program for Crystal Structure Determination," Cambridge Univ. Press, Cambridge, UK, 1976.
11. G. M. Sheldrick, *in* "Crystallographic Computing 3" (G. M. Sheldrick, C. Krüger, and R. Goddard Eds.), 175. Oxford Univ. Press, Oxford, 1985).

12. G. M. Sheldrick, "A Program for Crystal Structure Determination," University of Göttingen, 1993.
13. Diamond, "Visual Crystal Structure Information System" (G. Bergerhoff, Ed.), Gerhard-Domagk-Str.1, 53121 Bonn, Germany, 1996.
14. W. H. Zachariasen, *J. Less Common Met.* **62,** 1 (1978).
15. I. D. Brown, *in* "Structure and Bonding in Crystals" (O'Keeffe and Navrotsky, Eds.), Vol. 2, p. 1, Academic Press, San Diego, and references therein.
16. B. T. M. Willis and A. W. Pryor, "Thermal Vibrations in Crystallography," Cambridge Univ. Press, Cambridge, UK, 1975.
17. R. D. Shannon, *Acta Cryst. A* **32,** 751 (1976).
18. J. Mascetti, M. Vlasse, and C. Fouassier, *J. Solid State Chem.* **39,** 288 (1981).
19. L. Shirong, H. Qingzhen, Z. Yifan, J. Aidong, and C. Chuangtian, *Acta Cryst. C* **45,** 1861 (1989).
20. L. Mei, Y. Wang, and C. Chen, *Mat. Res. Bull.* **29,** 81 (1994).
21. H. Y.-P. Hong and K. Dwight, *Mat. Res. Bull.* **9,** 1661 (1974).
21a. A. Zalkin, J. D. Forrester, and D. H. Templeton, *Inorg. Chem.* **3,** 639 (1964).
22. J. D. Grice, J. Van Velthuizen, and R. A. Gault, *Can. Mineral.* **32,** 405 (1994).
23. B. R. Judd, *J. Chem. Phys.* **44,** 839 (1966).
24. N. Mercier, E. Antic-Fidancev, M. Lemaître-Blaise, and M. Leblanc, *J. Solid State Chem.* **132,** 33 (1997).
25. E. Antic-Fidancev, M. Lemaître-Blaise, J. P. Chaminade, and P. Porcher, *J. Alloys Comp.* **180,** 223 (1992).
26. J. Hölsä, *Inorg. Chim. Acta* **139,** 257 (1987).
27. G. Blasse, *Struct. Bonding* (*Berlin*) **26,** 43 (1976).
28. P. Porcher and P. Caro, *J. Chem. Phys.* **65,** 89 (1976).
29. F. Auzel and O. L. Malta, *J. Physique* **44,** 201 (1983).